

## Nonreciprocity through gain saturation in coupled nanocavities

Jianming Mai and Kok Wai Cheah <sup>\*</sup>

*Department of Physics, Hong Kong Baptist University, Kowloon Tong, Hong Kong SAR, China*

 (Received 19 June 2023; revised 13 November 2023; accepted 12 December 2023; published 2 January 2024)

The nonreciprocal properties of coupled nanocavities incorporating a gain medium were investigated. The proposed coupled nanocavities can be considered as a photonic non-Hermitian heterostructure. Our study shows that the nonlinearity arising from gain saturation plays a crucial role in dictating the transmittance characteristics. With increasing optical excitation intensity, the transmittance for the forward and backward incident directions exhibits a distinct evolution, ultimately leading to broken reciprocity. Furthermore, there exist both stable and metastable states of cavity modes, and these two states coalesce under a strong optical nonlinear effect. The coalescence of these two states can be attributed to the intricate interplay between the gain saturation nonlinearity and mode coupling, thus giving rise to different nonlinear optical characteristics. Our findings offer valuable insights into nonreciprocal phenomena such as optical bistability, and have potential applications for innovative devices with tunable optical properties.

DOI: [10.1103/PhysRevB.109.035101](https://doi.org/10.1103/PhysRevB.109.035101)

### I. INTRODUCTION

Nonreciprocity, viz., asymmetric received-transmitted field ratios between the exchangeable source(s) and detector(s) [1], is omnipresent in physics, such as acoustics [2–4], electronic circuits [5,6], and photonics [7–12]. As a typical way to realize nonreciprocity, nonlinear materials with electric field intensity-dependent permittivity can produce different permittivity responses under the asymmetric field distributions of the systems [13,14]. While the Kerr effect is a widely recognized source of nonlinearity, recently, gain saturation has offered an alternative insight for exploring nonreciprocal transmission [15–19]. Generally, a gain medium is employed to amplify the light intensity via stimulated emission. However, the output intensity does not increase limitlessly, as the field intensity affects the gain coefficient. Once the field intensity reaches a certain value, known as the saturation intensity of the gain materials, the amplification effect weakens [20,21].

By incorporating the gain saturation effect in non-Hermitian optical devices, there have been experimental demonstrations of nonreciprocal transmission in coupled cavities [22,23]. In addition, several studies have highlighted the optical bistability in coupled laser systems, facilitating the advancement of optical switching applications [24–26]. Nevertheless, the underlying mechanism and dynamic physical processes of nonreciprocal transmission and optical bistability in a coupled heterostructure with gain saturation effects still need to be explored in detail.

Here, we present a comprehensive investigation of the gain saturation nonlinearity that arises in gain media under different incident powers. First, the nonlinear coupled-mode theory (NCMT) equations are solved, revealing the intricate dynamic processes through which this type of nonlinearity influences

the optical characteristics of weak- and strong-coupled multilayer heterostructures. Then, our study demonstrates the concurrent achievement of nonreciprocal transmission and optical bistability via both a theoretical analysis and simulations. The findings of this research show considerable potentials for various applications, including all-optical quantum computation, communication systems, and time-modulated optical pump-probe experiments [27,28].

### II. THEORY

To investigate the gain saturation in a non-Hermitian coupled cavity system, we design a multilayer thin-film heterostructure as illustrated in Fig. 1. The structure comprises five layers, denoted from top to bottom as  $l_1$ ,  $l_2$ ,  $l_3$ ,  $l_4$ , and  $l_5$ , with respective thicknesses  $L_1$ ,  $L_2$ ,  $L_3$ ,  $L_4$ , and  $L_5$ . In our configuration  $l_1$ ,  $l_3$ , and  $l_5$  are silver layers, whereas  $l_2$  serves as the gain material and  $l_4$  is the passive dielectric layer with refractive indices  $n_2$  and  $n_4$ , respectively. When the incident power is too weak to trigger a significant change in permittivity ( $\Delta \varepsilon/\varepsilon \leq 10^{-4}$ ), the gain saturation nonlinearity can be neglected. In this case we assume that the system is in a linear regime. When  $\Delta \varepsilon/\varepsilon > 10^{-4}$ , the system is in a nonlinear regime. Furthermore, we define the forward incidence as light propagating from  $l_1$  to  $l_5$ , while the backward incidence corresponds to light traveling from the opposite direction. The light is confined within layers  $l_2$  and  $l_4$  by the silver layers, so the proposed structure can be conceptualized as a pair of Fabry-Pérot microcavities with resonant frequencies  $\omega_a$  and  $\omega_b$ . To simplify the calculation, let  $\omega_a = \omega_b$ , and the decay rates of two microcavities are designated as  $Y_a$  and  $Y_b$ . The coupling strength  $\kappa$  between the two microcavities is determined by the thickness of layer  $L_3$  [29]. In both a theoretical analysis and simulations, the silver layers can be described by the Drude model, where the high-frequency dielectric constant is 3.7, the plasma frequency is  $2.2 \times 10^{15}$  Hz, and the

<sup>\*</sup>Corresponding author: kwcheah@hkbu.edu.hk

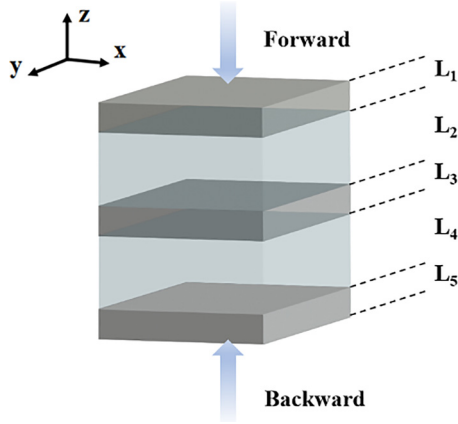


FIG. 1. Schematic of the multilayer thin-film heterostructure. Each layer from the top view side to bottom is denoted as  $l_1, l_2, l_3, l_4,$  and  $l_5$ , respectively, in which  $l_1, l_3,$  and  $l_5$  are the silver,  $l_2$  is the gain layer, and  $l_4$  is the passive dielectric layer. Light incident from  $l_1$  is defined as forward incident while from  $l_5$  it is defined as backward incident.

damping coefficient equals  $4.3524 \times 10^{12}$  Hz [30]. Also,  $n_4 = 1.5$ ,  $L_1 = L_5 = 30$  nm,  $L_3 = 80$  nm, and  $L_2 = L_4 = 800$  nm. When  $L_3 = 80$  nm, there is weak coupling between the two nanocavities leading to a single common resonant mode [29], while strong coupling is achieved with thinner  $L_3$ , and is described in the Supplemental Material (SM) [31]. The light is set as normal incident. Due to the complex permittivity of silver in the optical range, the system is non-Hermitian [32].

In the steady state, the complex field amplitudes  $\tilde{a}$  and  $\tilde{b}$  of light in coupled cavities can be described by nonlinear equations of motion. For the proposed heterostructure it can be expressed in the frequency domain as [23,33]

$$\begin{pmatrix} \omega - \omega_a + i\gamma_a - i\frac{g_0}{2(1+\frac{|\tilde{a}|^2}{I_{\text{sat}}})} & -\kappa \\ -\kappa & \omega - \omega_b + i\gamma_b \end{pmatrix} \begin{pmatrix} \tilde{a} \\ \tilde{b} \end{pmatrix} = \begin{pmatrix} e_1 \\ e_2 \end{pmatrix}, \quad (1)$$

in which  $g_0$  is the small-signal gain,  $I_{\text{sat}}$  is the gain saturation intensity, and  $\gamma_{a(b)} = Y_{a(b)}/2$ . Here,  $g_0$  is set as  $10^{14}$  and  $I_{\text{sat}}$  is  $2.5 \times 10^{27}$ . For forward incidence  $e_1 = -i\sqrt{\kappa_{ea}}f^{\text{in}}$  and  $e_2 = 0$ , whereas for backward incidence  $e_1 = 0$  and  $e_2 = -i\sqrt{\kappa_{eb}}b^{\text{in}}$ , where  $f^{\text{in}}$  and  $b^{\text{in}}$  are the incident light fields of the forward and backward incident directions, respectively,  $\kappa_{ea(eb)}$  is the loss rate for the coupling between cavity  $a(b)$  and the environment, and  $i^2 = -1$ . The incident power of two incident directions is defined as  $P_{\text{in}} = |f_{\text{in}}|^2 = |b_{\text{in}}|^2$ .

For the NCMT, the transmittance  $T^{\text{nl}}$  is proportional to  $|\chi_t^{\text{nl}}|^2$  [34],

$$T^{\text{nl}} = |t^{\text{nl}}|^2 \propto |\chi_t^{\text{nl}}|^2, \quad (2)$$

in which  $t^{\text{nl}}$  represent the transmission coefficient, and

$$\chi_t^{\text{nl}} = \frac{-\kappa}{\left(\omega - \omega_a + i\gamma_a - i\frac{g_0}{2(1+\frac{|\tilde{a}|^2}{I_{\text{sat}}})}\right)(\omega - \omega_b + i\gamma_b) - \kappa^2}. \quad (3)$$

Thus, the transmittance from  $|\chi_t^{\text{nl}}|^2$  can be derived. Due to the difference of  $\tilde{a}$  of forward and backward incidence,  $|\chi_t^{\text{nl}}|^2$  of

forward ( $|\chi_{tf}^{\text{nl}}|^2$ ) and backward ( $|\chi_{tb}^{\text{nl}}|^2$ ) are not the same, which causes nonreciprocal transmission in the nonlinear regime of the system.

By solving Eqs. (1) and (3) under different normalized incident powers with  $n_2 = 1.5$ , we calculate  $|\chi_{tf}^{\text{nl}}|^2$  and  $|\chi_{tb}^{\text{nl}}|^2$ , represented by a red solid circle and black open circle, respectively, as depicted in Fig. 2. From Fig. 2 the solutions of both  $|\chi_{tf}^{\text{nl}}|^2$  and  $|\chi_{tb}^{\text{nl}}|^2$  exist in two states. One is the balloon-shaped state, whereas the other one is the continuous state. Here, we define them as metastable and stable states, respectively. As the normalized incident power increases from 0.02 to 0.33, the two stable states experience a transition whereby they initially appear indistinguishable, but progressively, the forward gradually exceeds the backward. Concurrently, the higher values of two metastable states decrease and approach that of the stable states. Notably, the black balloon (backward) exhibits a more pronounced decline, ultimately intersecting the red balloon (forward), as depicted in Figs. 2(a)–2(c). In Fig. 2(d) at  $P_{\text{in}} = 0.45$ , the two separate states of  $|\chi_{tf}^{\text{nl}}|^2$  merge, resulting in a sudden jump up in the  $|\chi_{tf}^{\text{nl}}|^2$  value at the merging points ( $\lambda = 425.3$  nm and  $\lambda = 427.1$  nm), while the two states of  $|\chi_{tb}^{\text{nl}}|^2$  remain separated. At a higher incident power of  $P_{\text{in}} = 0.75$  [Fig. 2(e)], the black balloon and its corresponding stable state of  $|\chi_{tb}^{\text{nl}}|^2$  merge. In the region between the merging points,  $|\chi_{tb}^{\text{nl}}|^2$  is larger than  $|\chi_{tf}^{\text{nl}}|^2$ , attributable to the higher values of the black balloon. Finally, the difference between  $|\chi_{tf}^{\text{nl}}|^2$  and  $|\chi_{tb}^{\text{nl}}|^2$  tends to reach an equilibrium when the incident power causes the separated states of both forward and backward incidence to merge, as illustrated in Fig. 2(f) where  $P_{\text{in}} = 1.1$ .

We further study the characteristics of  $|\chi_{tf}^{\text{nl}}|^2$  and  $|\chi_{tb}^{\text{nl}}|^2$  independently, where  $n_2 = 1.5$  with the normalized incident power at  $\lambda = 426.7$  nm (Fig. 3). From Fig. 2, in the wavelength domain the bistability can be found where the balloon appears. The red solid line represents  $|\chi_{tf}^{\text{nl}}|^2$ , while the black solid line represents  $|\chi_{tb}^{\text{nl}}|^2$ . From Fig. 3, we can see that both the red and black curves have three branches, indicative of bistable behavior, in which the middle and the upper branches exhibit steep gradient branches. Owing to the instability of the middle branches, abrupt increases and drops are observed at the endpoints of the upper and lower branches, as indicated by the red and black dashed arrows. These endpoints are defined as up and down thresholds, respectively. Consequently, the bistable width is the disparity between the up and down thresholds. In addition, despite the similar shapes, the black curve exhibits a more extensive bistable width compared to the red curve, with its up threshold occurring at a higher power value. This also corresponds to the higher values of the black balloon relative to the red balloon in Fig. 2.

### III. RESULTS AND DISCUSSIONS

To elucidate further the optical response of the proposed structure, we perform a simulation using COMSOL MULTI-PHYSICS. In the simulation, we use the continuous wave (CW) as the excitation. The refractive index of a material can be expressed as  $n = n_r \mp ik$ , where the  $\mp$  indicates whether the material is gain or loss, and the amount of gain or loss is reflected by the non-Hermiticity component  $k$ . To consider the nonlinearity effect of the gain material from gain saturation,

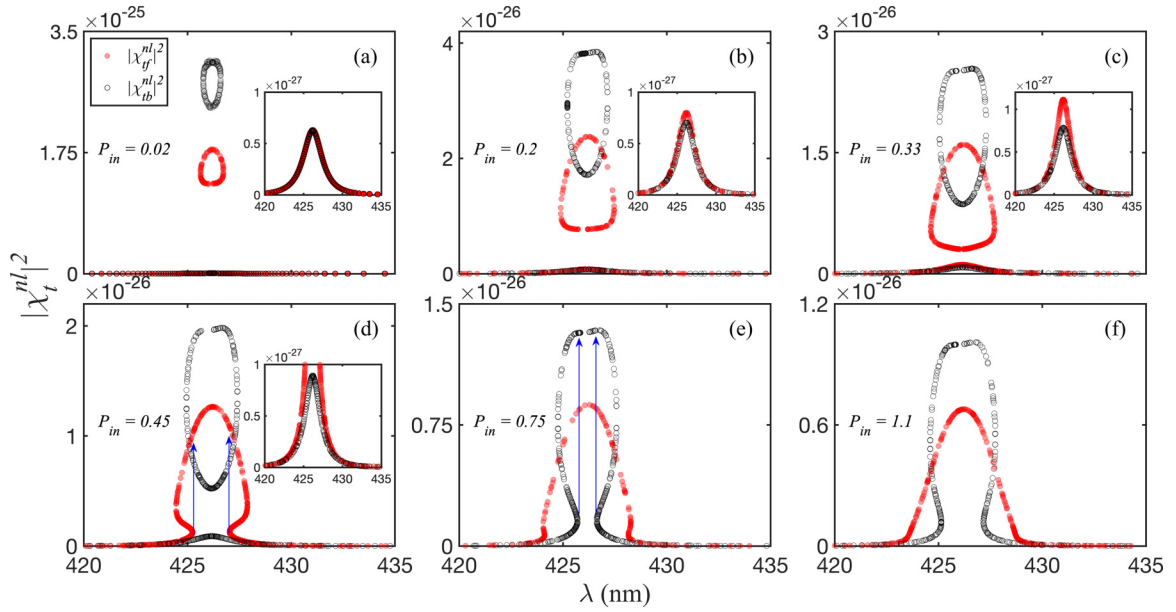


FIG. 2.  $|\chi_f^{nl}|^2$  of forward  $|\chi_{rf}^{nl}|^2$  and backward  $|\chi_{tb}^{nl}|^2$  incidence at (a)  $P_{in} = 0.02$ , (b)  $P_{in} = 0.2$ , (c)  $P_{in} = 0.33$ , (d)  $P_{in} = 0.45$ , (e)  $P_{in} = 0.75$ , and (f)  $P_{in} = 1.1$ . The red solid circle stands for the  $|\chi_{rf}^{nl}|^2$ , whereas the black open circle stands for the  $|\chi_{tb}^{nl}|^2$ . The inset boxes in (a)–(d) present an enlarged view of the stable states.

the complex permittivity of gain materials can be written as [35]

$$\varepsilon = n_r^2 + \frac{-k^2 - 2ikn_r}{1 + \frac{|E|^2}{|E_{sat}|^2}}, \quad (4)$$

in which  $|E|$  is the electric field within the gain medium, whereas  $|E_{sat}|^2$  is the saturation field intensity associated with the gain material. In the simulation, the refractive index in  $l_2$  is set as  $n_2 = 1.5 - 0.015i$  with  $E_{sat}$  assumed as  $=10^7$  V/m [36].

We obtain the transmittance in arbitrary units (a.u.) of forward and backward incidence under different incident powers, in Fig. 4, in which the red solid lines stand for forward incidence, whereas the black dashed lines stand for backward incidence. When the incident power increases from  $0.005$  GW/cm<sup>2</sup> [Fig. 4(a)] to  $0.375$  GW/cm<sup>2</sup> [Fig. 4(c)],

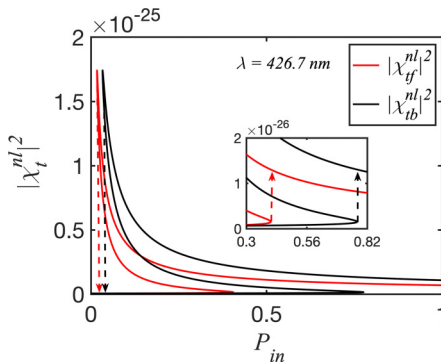


FIG. 3. Optical bistability of  $|\chi_{rf}^{nl}|^2$  and  $|\chi_{tb}^{nl}|^2$  with the normalized incident power  $P_{in}$  at  $\lambda = 426.7$  nm. The inset box presents an enlarged view of the up thresholds.

the transmittances of both forward and backward incidence exhibit a slight increase, with the forward transmittance being progressively greater than the backward one due to the considerable influence by the nonlinear effect. The characteristics of the transmittance curves in Figs. 4(a)–4(c) are well consistent with the stable states presented in Figs. 2(a)–2(c). Furthermore, this suggests that prior to the merging of the two states the metastable states are unobservable, so only the stable states can be observed. When compared with Figs. 4(a)–4(c) the forward transmittance in Fig. 4(d), viz.,  $P_{in} = 0.425$  GW/cm<sup>2</sup>, has an abrupt 6.5 times increase at  $\lambda = 426.3$  nm, while the backward transmittance remains at a relatively low value of  $\sim 1.65$ . This transformation can be attributed to the merging of the red “balloon” with the stable state, causing the metastable state to become observable between the two merging points. Consequently, the transmittance experiences an abrupt increase, and the forward transmittance curve assumes a narrow columnar shape at the two merging points, as indicated by the blue arrows in Fig. 2(d). However, a similar transformation for backward transmittance occurs at  $P_{in} = 1.1$  GW/cm<sup>2</sup>, causing the backward transmittance to in turn exceed that of the forward [Fig. 4(e)]. Figure 5 shows the electric field distribution of forward (red curves) and backward (black curves) incidence ( $\lambda = 426.3$  nm) along the  $z$  direction with different incident power values that are sufficiently intense to induce significant nonreciprocity. When  $P_{in} = 0.425$  GW/cm<sup>2</sup> [Fig. 5(a)], the output field of forward incidence is higher than that of backward incidence. In contrast, when  $P_{in}$  increases to  $P_{in} = 1.1$  GW/cm<sup>2</sup> [Fig. 5(b)], the backward output field is higher. The field distribution results are similarly reflected in Figs. 4(d) and 4(e). At a higher incident power at  $P_{in} = 1.5$  GW/cm<sup>2</sup>, both transmittance curves settle into their respective steady shape, as shown in Fig. 4(f).

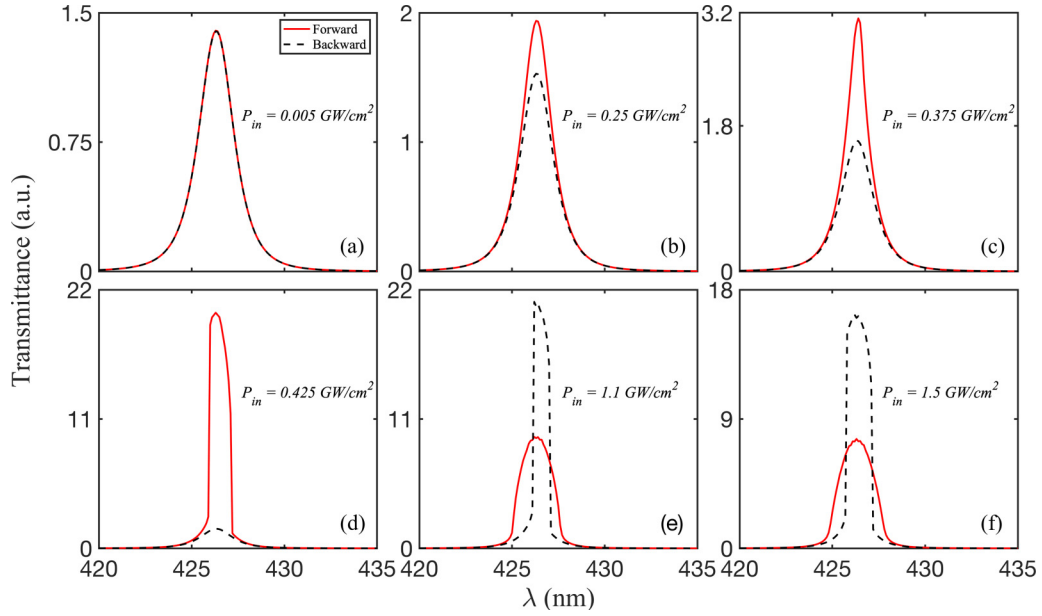


FIG. 4. Transmittance of forward (red solid line) and backward (black dashed line) incidence when (a)  $P_{in} = 0.005 \text{ GW/cm}^2$ , (b)  $P_{in} = 0.25 \text{ GW/cm}^2$ , (c)  $P_{in} = 0.375 \text{ GW/cm}^2$ , (d)  $P_{in} = 0.425 \text{ GW/cm}^2$ , (e)  $P_{in} = 1.1 \text{ GW/cm}^2$ , and (f)  $P_{in} = 1.5 \text{ GW/cm}^2$ .

Additionally, in the simulation the dependence of the incident power of optical bistability at  $\lambda = 426.5 \text{ nm}$  in the transmittance of forward and backward incidence is obtained. In Fig. 6, the red/black curves are the forward/backward transmittance, where the cross-marker (circle-marker) curves stand for the gradually increasing (decreasing) step. In each simulation step, the incident power is calculated according to the incident power from the previous step. For increasing steps

(viz., incident power), the red and black cross-marker curves have a sudden increase at  $0.39$  and  $1.078 \text{ GW/cm}^2$ , respectively, which are the up thresholds for forward and backward incidence. Conversely, for the decreasing step, the transmittance for the two incidences decreases abruptly from about  $256$  to  $1.4$  at the down thresholds:  $0.021$  and  $0.057 \text{ GW/cm}^2$ , respectively. The asymmetric increase and decrease thresholds give rise to a bistable loop in transmittance. As a result of distinct cavity field amplitudes and weak coupling for the two cavities, the backward incidence necessitates a higher power to achieve an equivalent gain saturation effect in cavity  $a$  as compared to the forward incidence, which leads to a larger bistable width for backward incidence. The simulation outcomes, including the dynamic processes across the wavelength domain and optical bistability about the incident powers, exhibit excellent agreement with the theoretical analysis in Sec. II.

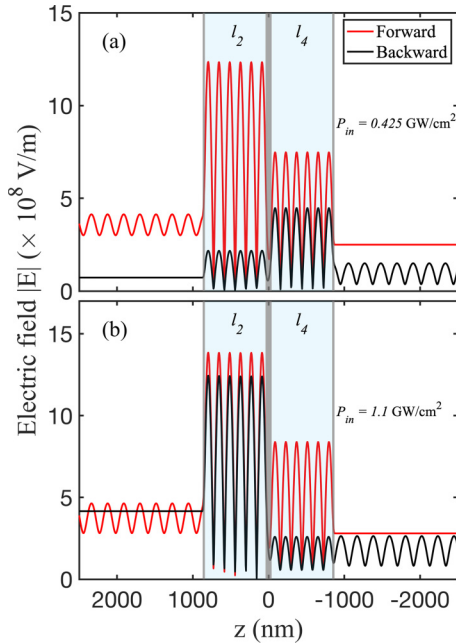


FIG. 5. Electric field distribution along the  $z$  direction at  $\lambda = 426.3 \text{ nm}$  when (a)  $P_{in} = 0.425 \text{ GW/cm}^2$  and (b)  $P_{in} = 1.1 \text{ GW/cm}^2$ . The forward incidence is in red, while the backward incidence is in black.  $l_1$ ,  $l_3$ , and  $l_5$  are the gray-shaded areas, respectively. The light-blue-shaded regions are  $l_2$  and  $l_4$ .

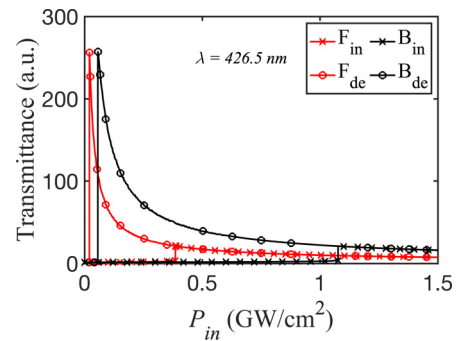


FIG. 6. Optical bistability of forward (red) and backward (black) incidence with the incident power  $P_{in}$  at  $\lambda = 426.5 \text{ nm}$ . The red and black cross-marker lines are obtained by gradually increasing power, whereas the red and black circle-marker lines are obtained by gradually decreasing power.

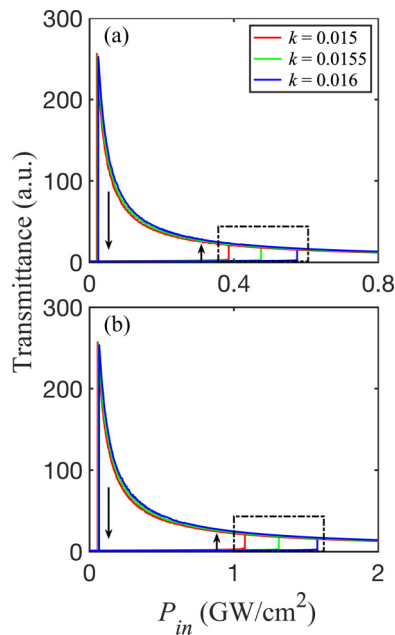


FIG. 7. Optical bistability loops at  $\lambda = 426.5$  nm, with gradually increasing power (indicated by upward arrows) and decreasing power (indicated by downward arrows) simulation steps, and different  $k$  of (a) forward and (b) backward incidence. The red, green, and blue curves represent  $k = 0.015$ ,  $0.0155$ , and  $0.016$ , respectively.

Figures 7(a) and 7(b) show optical bistability loops at  $\lambda = 426.5$  nm, with gradually increasing power (indicated by upward arrows) and decreasing power (indicated by downward arrows) simulation steps, and different  $k$  for forward and backward incidence. Bistability loops with higher  $k$  values have larger up and down thresholds. Compared with forward incidence, the bistability loops of backward incidence have larger thresholds. Moreover, the differences in the up thresholds (highlighted by the rectangular frame) are more significant.

#### IV. CONCLUSION

In this paper, we show that nonreciprocity can be achieved in coupled nanocavities when one of the dielectric layers is a gain medium. Both nonreciprocal transmission and optical bistability in the coupled heterostructure are driven by gain saturation nonlinearity. By solving the NCMT, we have uncovered the dynamic processes that govern the optical characteristics over a range of incident powers. Optical bistability arises from the merging of stable and metastable states, while nonreciprocity emerges due to the distinct merging threshold powers required for forward and backward incidence. As incident power increases, the metastable state progressively approaches the stable ones, and once reaching a particular power value, two states coalesce. This leads to a sudden increase in the transmission spectra as the metastable state becomes observable after merging with the stable state. In addition, under weak coupling the metastable state of backward incidence appears at a higher incident power than the forward incidence, thereby precipitating the nonreciprocal transmission of the system, whereas the two splitting modes under strong coupling have higher values of the metastable state for forward incidence. Our results demonstrate the significant role of gain saturation nonlinearity in governing the transmittance of light for both forward and backward incident directions as the incident power becomes dominant. The good agreement between the theoretical analysis and simulations reinforces the validity of our findings and their implications for understanding the intricate interplay of nonlinearity and mode coupling in such photonic systems.

#### ACKNOWLEDGMENT

This work is supported by Hong Kong Research Grant Council Research Grant No. AoE/P-02/12.

- [1] C. Caloz, A. Alù, S. Tretyakov, D. Sounas, K. Achouri, and Z.-L. Deck-Léger, Electromagnetic nonreciprocity, *Phys. Rev. Appl.* **10**, 047001 (2018).
- [2] X. Zhu, J. Li, C. Shen, X. Peng, A. Song, L. Li, and S. A. Cummer, Non-reciprocal acoustic transmission via space-time modulated membranes, *Appl. Phys. Lett.* **116**, 034101 (2020).
- [3] H. Nassar, B. Yousefzadeh, R. Fleury, M. Ruzzene, A. Alù, C. Daraio, A. N. Norris, G. Huang, and M. R. Haberman, Nonreciprocity in acoustic and elastic materials, *Nat. Rev. Mater.* **5**, 667 (2020).
- [4] L. Shao, W. Mao, S. Maity, N. Sinclair, Y. Hu, L. Yang, and M. Loñcar, Non-reciprocal transmission of microwave acoustic waves in nonlinear parity-time symmetric resonators, *Nat. Electron.* **3**, 267 (2020).
- [5] A. Nagulu, N. Reiskarimian, and H. Krishnaswamy, Non-reciprocal electronics based on temporal modulation, *Nat. Electron.* **3**, 241 (2020).
- [6] N. A. Estep, D. L. Sounas, J. Soric, and A. Alù, Magnetic-free nonreciprocity and isolation based on parametrically modulated coupled-resonator loops, *Nat. Phys.* **10**, 923 (2014).
- [7] D. L. Sounas and A. Alù, Non-reciprocal photonics based on time modulation, *Nat. Photon.* **11**, 774 (2017).
- [8] L. Feng, M. Ayache, J. Huang, Y.-L. Xu, M.-H. Lu, Y.-F. Chen, Y. Fainman, and A. Scherer, Nonreciprocal light propagation in a silicon photonic circuit, *Science* **333**, 729 (2011).
- [9] A. M. Shaltout, V. M. Shalaev, and M. L. Brongersma, Spatiotemporal light control with active metasurfaces, *Science* **364**, eaat3100 (2019).
- [10] A. Li and W. Bogaerts, Reconfigurable nonlinear nonreciprocal transmission in a silicon photonic integrated circuit, *Optica* **7**, 7 (2020).
- [11] L. Bi, J. Hu, P. Jiang, D. H. Kim, G. F. Dionne, L. C. Kimmerling, and C. Ross, On-chip optical isolation in monolithically integrated non-reciprocal optical resonators, *Nat. Photon.* **5**, 758 (2011).
- [12] D. L. Sounas and A. Alù, Time-reversal symmetry bounds on the electromagnetic response of asymmetric structures, *Phys. Rev. Lett.* **118**, 154302 (2017).
- [13] D. Jalas, A. Petrov, M. Eich, W. Freude, S. Fan, Z. Yu, R. Baets, M. Popović, A. Melloni, J. D. Joannopoulos *et al.*, What

- is—and what is not—an optical isolator, *Nat. Photon.* **7**, 579 (2013).
- [14] S. Fan, R. Baets, A. Petrov, Z. Yu, J. D. Joannopoulos, W. Freude, A. Melloni, M. Popović, M. Vanwolleghem, D. Jalas *et al.*, Comment on “Nonreciprocal light propagation in a silicon photonic circuit”, *Science* **335**, 38 (2012).
- [15] K. Y. Yang, J. Skarda, M. Cotrufo, A. Dutt, G. H. Ahn, M. Sawaby, D. Vercruyssen, A. Arbabian, S. Fan, A. Alù *et al.*, Inverse-designed non-reciprocal pulse router for chip-based lidar, *Nat. Photon.* **14**, 369 (2020).
- [16] Y. Shi, Z. Yu, and S. Fan, Limitations of nonlinear optical isolators due to dynamic reciprocity, *Nat. Photon.* **9**, 388 (2015).
- [17] A. B. Khanikaev and A. Alù, Nonlinear dynamic reciprocity, *Nat. Photon.* **9**, 359 (2015).
- [18] D. L. Sounas, J. Soric, and A. Alù, Broadband passive isolators based on coupled nonlinear resonances, *Nat. Electron.* **1**, 113 (2018).
- [19] C. Li, S.-Y. Wu, and J.-F. Wu, Broad-band, reversible non-reciprocal light transmission based on a single nanocavity, *Opt. Express* **27**, 16530 (2019).
- [20] S. Vashahri-Ghamsari, B. He, and M. Xiao, Effects of gain saturation on the quantum properties of light in a non-Hermitian gain-loss coupler, *Phys. Rev. A* **99**, 023819 (2019).
- [21] Y. F. Xie, Z. Cao, B. He, and Q. Lin, Pt-symmetric phonon laser under gain saturation effect, *Opt. Express* **28**, 22580 (2020).
- [22] B. He, L. Yang, X. Jiang, and M. Xiao, Transmission nonreciprocity in a mutually coupled circulating structure, *Phys. Rev. Lett.* **120**, 203904 (2018).
- [23] L. Chang, X. Jiang, S. Hua, C. Yang, J. Wen, L. Jiang, G. Li, G. Wang, and M. Xiao, Parity-time symmetry and variable optical isolation in active-passive-coupled microresonators, *Nat. Photon.* **8**, 524 (2014).
- [24] H. Wang, S. Assaworranit, and S. Fan, Dynamics for encircling an exceptional point in a nonlinear non-Hermitian system, *Opt. Lett.* **44**, 638 (2019).
- [25] Z. Gao, S. T. Fryslie, B. J. Thompson, P. S. Carney, and K. D. Choquette, Parity-time symmetry in coherently coupled vertical cavity laser arrays, *Optica* **4**, 323 (2017).
- [26] X.-W. Ma, Y.-Z. Huang, Y.-D. Yang, H.-Z. Weng, F.-L. Wang, M. Tang, J.-L. Xiao, and Y. Du, All-optical flip-flop based on hybrid square-rectangular bistable lasers, *Opt. Lett.* **42**, 2291 (2017).
- [27] R. Tirole, S. Vezzoli, E. Galiffi, I. Robertson, D. Maurice, B. Tilmann, S. A. Maier, J. B. Pendry, and R. Sapienza, Double-slit time diffraction at optical frequencies, *Nat. Phys.* **19**, 999 (2023).
- [28] R. Tirole, E. Galiffi, J. Dranczewski, T. Attavar, B. Tilmann, Y.-T. Wang, P. A. Huidobro, A. Alù, J. B. Pendry, S. A. Maier *et al.*, Saturable time-varying mirror based on an epsilon-near-zero material, *Phys. Rev. Appl.* **18**, 054067 (2022).
- [29] J. Mai, Y. Chen, G. Li, and K. W. Cheah, Double exceptional points in grating coupled metal-insulator-metal heterostructure, *Opt. Express* **30**, 40053 (2022).
- [30] P. B. Johnson and R.-W. Christy, Optical constants of the noble metals, *Phys. Rev. B* **6**, 4370 (1972).
- [31] See Supplemental Material at <http://link.aps.org/supplemental/10.1103/PhysRevB.109.035101> for the details of nonreciprocal transmission and bistability induced by gain saturation under strong coupling, including analytical calculations and simulation results.
- [32] J. Yim, H. Zhao, B. Midya, and L. Feng, Non-Hermitian heterostructure for two-parameter sensing, *Opt. Lett.* **44**, 1626 (2019).
- [33] A. K. Jahromi, A. U. Hassan, D. N. Christodoulides, and A. F. Abouraddy, Statistical parity-time-symmetric lasing in an optical fibre network, *Nat. Commun.* **8**, 1359 (2017).
- [34] J. Mai and K. W. Cheah, Nonreciprocal transmission in a nonlinear coupled heterostructure, *Opt. Express* **30**, 46357 (2022).
- [35] D. R. Barton, H. Alaeian, M. Lawrence, and J. Dionne, Broadband and wide-angle nonreciprocity with a non-Hermitian metamaterial, *Phys. Rev. B* **97**, 045432 (2018).
- [36] M. P. H. Andresen, A. V. Skaldebo, M. W. Haakestad, H. E. Krogstad, and J. Skaar, Effect of gain saturation in a gain compensated perfect lens, *J. Opt. Soc. Am. B* **27**, 1610 (2010).